INTERNATIONAL JOURNAL FOR NUMERICAL AND ANALYTICAL METHODS IN GEOMECHANICS
Int. J. Numer. Anal. Meth. Geomech., **23**, 335–354 (1999)

MODELLING OF SUBMARINE LANDSLIDES OF ROCK AND SOIL

C. MARIOTTI* AND P. HEINRICH

Laboratoire de Détection et de Géophysique, Commissariat à l'Energie Atomique, B.P. 12, 91680 Bruyères-le-Châtel, France

SUMMARY

Landslides and their hydraulic effects are studied by numerical and experimental means. A two-dimensional model based on Navier–Stokes equations has been developed considering the sediments and water as a mixture. A Bingham law written in effective stress and an erosion–diffusion law at the water–sediment interface have been introduced into the model. Laboratory experiments consisting in the sliding of a block, a coarse gravel and a fine sand have been carried out. The results are compared with the numerical model. These experiments show the importance of sediment rheology and interstitial pressure in slide velocity and water wave generation. Copyright © 1999 John Wiley & Sons, Ltd.

Key words: submarine landslides; incompressible viscous fluid; Bingham fluid

1. INTRODUCTION

Underwater landslides, most commonly induced by the oversteepening of a slope or by the liquefaction of sediments, can generate small-scale tsunamis in coastal areas. This type of tsunami can produce large run-up heights on the coast.

The sliding of these unstable sedimentary bodies can generate water waves that are destructive for coastal areas[1–4] or for specific constructions like dams.

Few studies have been done regarding the interaction between an underwater landslide and the generated surface waves. Recently, Jiang and Leblond[5] developed a numerical fluid model to simulate the coupling of a submarine landslide on a gentle uniform slope with the generated surface waves. The landslide is treated as a laminar flow of incompressible viscous and Bingham plastic fluids. Long-wave approximation is adopted for both water waves and mudslide. However, the long-wave approximation is often inaccurate for steep slopes.

We propose to solve the complete Navier–Stokes equations considering sediments and ambient water as a mixture. The behaviour of sediments is treated using an effective stress Bingham law and an erosion–diffusion at the water–sediment interface. Tank experiments of submarine sliding are described and compared with the numerical results.

*Correspondence to: Christian Mariotti, CEA/DAM/DASE, Laboratoire de Détection et de Géophysique, Centre de Bruyéres le Chatel, B.P. 12-91680 Bruyères-le-Châtel, France

Contract grant sponsor: DG XII of the Commission of the European Communities with the project GITEC

CCC 0363–9061/99/040335–20$17.50

Received 26 September 1997
Revised 21 April 1998

2. NUMERICAL MODEL: Nasa-Vof2D AND ITS EXTENSIONS

Submarine landslides are simulated by means of a two-dimensional mixture model based on the Navier–Stokes equations.

In order to model coupling between sediments and water waves, the two-dimensional hydrodynamics program Nasa-Vof2D,[6] developed by Torrey *et al.* in 1985, has been transformed into a 'diffusion' model. Rheological laws have been introduced to simulate the mechanical behaviour of the sediments and the shear stress has been added to the initial Navier–Stokes equations.

The Eulerian program Nasa-Vof2D solves the complete incompressible and non-linear Navier–Stokes equations for one single fluid with a free surface and simulates flows around fixed obstacles.

The concept of the 'diffusion' model is to consider saturated sediments and water of the tank as a mixture, rather than two phases separately.[7,8] The new version of the model is then expressed in terms of two mixture equations of conservation of mass and momentum, an equation of water surface and one additional erosion–diffusion equation, which takes into account the concentration changes. Like for the water of the tank, the saturated soil is considered incompressible. The mixture is then incompressible. But in reality, the solid skeleton of a soil is compressible. When loaded, either the interstitial water experiences a relative displacement with respect to the solid skeleton under drained conditions or the interstitial pressure changes. This phenomenon is taken into account by assuming the effective stress principle in the modelling of sandflows.

The non-linear governing equations for the mixture are

the continuity equation for each phase:

$$\frac{\partial c\rho_{\text{sat}}}{\partial t} + \nabla\cdot(c\rho_{\text{sat}}\mathbf{v}_{\text{sat}}) = 0 \tag{1}$$

$$\frac{\partial (1-c)\rho_{\text{w}}}{\partial t} + \nabla\cdot((1-c)\rho_{\text{w}}\mathbf{v}_{\text{w}}) = 0 \tag{2}$$

with the volumetric concentration c of the saturated soil, the two field velocity variables $\mathbf{v}_{\text{sat}}$ and $\mathbf{v}_{\text{w}}$, the water density ρ_{w} and the saturated density of the soil ρ_{sat}. A unit value of c corresponds to the saturated soil and a zero value of c indicates the water of the tank. This concentration c is variable in space and time.

The density ρ_{sat} is defined by the porosity n and the gain density ρ_{s}:

$$\rho_{\text{sat}} = n\rho_{\text{w}} + (1-n)\rho_{\text{s}} \tag{3}$$

Taking each phase separately, the incompressibility is defined by the constant value of ρ_{w} and ρ_{sat} resulting in the following equation for the volumetric mean velocity:

$$\nabla\cdot((1-c)\mathbf{v}_{\text{w}} + c\mathbf{v}_{\text{sat}}) = 0 \tag{4}$$

But assuming the mixture, the mean velocity of the mixture $\mathbf{v}$ is defined by the densities of the phases and the density of the mixture ρ as

$$\rho\mathbf{v} = c\rho_{\text{sat}}\mathbf{v}_{\text{sat}} + (1-c)\rho_{\text{w}}\mathbf{v}_{\text{w}} \tag{5}$$

$$\rho = c\rho_{\text{sat}} + (1-c)\rho_{\text{w}} \tag{6}$$

resulting in the continuity equation

$$\frac{\partial \rho}{\partial t} + \nabla \cdot (\rho \mathbf{v}) = 0 \tag{7}$$

and the momentum equation

$$\frac{\partial \rho \mathbf{v}}{\partial t} + \nabla \cdot \rho \mathbf{v}\mathbf{v} = \rho \mathbf{g} - \nabla p + \nabla \cdot \tau \tag{8}$$

where p, τ and $\mathbf{g}$ are, respectively, the pressure, the shear stress tensor and the gravitational acceleration vector.

The fractional volume F of the cell occupied by the mixture at the water surface is used to calculate the water–air interface by solving the following equation:

$$\frac{\partial F}{\partial t} + \nabla \cdot (F \mathbf{v}) = 0 \tag{9}$$

The conservation of mass of the saturated soil is linked to the relative velocity between the mixture and the saturated soil by the relation

$$\frac{\partial c\rho_{\text{sat}}}{\partial t} + \nabla \cdot (c\rho_{\text{sat}} \mathbf{v}) = \nabla \cdot (c\rho_{\text{sat}} [\mathbf{v} - \mathbf{v}_{\text{sat}}]) = -\nabla \cdot \mathbf{j} \tag{10}$$

where $\mathbf{j}$ is the erosion–diffusion flux.

In the model, $\mathbf{j}$ is given by a law and $\mathbf{v}$ is calculated, therefore the velocity $\mathbf{v}_{\text{sat}}$ is not calculated. Sediment suspensions in marine environment are generally modelled using the concept of gradient diffusion[9] with $\mathbf{j}$ modelled as follows by Fick's law:

$$\mathbf{j} = -D \nabla c \tag{11}$$

where in our applications the sediment diffusivity D has been chosen constant for simplicity.

3. RHEOLOGICAL MODEL OF THE DENSE PART

The Bingham viscoplastic model, in which no strain occurs until a specified shear stress is applied at the dense part, is used. It is widely employed to describe the behaviour law of these sediments by combining the yield stress τ_0, also called the Bingham yield, and the plastic dynamic viscosity μ_b. These non-Newtonian fluids[10] are also called generalized Newtonian fluids with a viscosity $\mu(\dot{\bar{\varepsilon}})$. The relation between the shear stress τ and the shear strain rate $\dot{\bar{\varepsilon}}$ is expressed by

$$\tau = \mu(\dot{\bar{\varepsilon}}) \dot{\bar{\varepsilon}} \tag{12}$$

$$\mu(\dot{\bar{\varepsilon}}) = \begin{cases} \mu_b + \dfrac{\tau_0}{\sqrt{\dot{\bar{\varepsilon}} : \dot{\bar{\varepsilon}}}} & \text{if } \dfrac{1}{2} \tau : \tau \geqslant \tau_0^2 \\ \infty \text{ and } \dot{\bar{\varepsilon}} = 0 & \text{if } \dfrac{1}{2} \tau : \tau \leqslant \tau_0^2 \end{cases}$$

where

$$\mathbf{A} : \mathbf{A} = A_{ij} A_{ji} \tag{13}$$

τ_0 is an initial yield which can be initialized in space to take into account the static equilibrium or some variability of the geometrial properties. During the calculation, this yield associated with the concentration c is convected in relation with the displacement of the dense part in the Eulerian grid:

$$\frac{\partial \tau_0 c}{\partial t} + \nabla \cdot (\tau_0 c \mathbf{v}) = 0 \tag{14}$$

4. EXPERIMENTION A ROCK SLIDE

To validate the developments made, we have simulated submarine sliding of a rigid block in tank tests. This experiment[11] consists in generating water waves by allowing a rigid block to slide freely down a frictionless inclined plane with a slope of 45°. The channel is 20 m long, 0.55 m wide and 1.50 m high. The rigid block, with a specific gravity of 2, is a triangle of length of 0.50 m. The water depth is 1.00 m and the top of the triangular mass is initially 1 cm below the water surface.

The computational domain in 5·0 m by 1·30 m in the x and y directions. The grid consists of 300 columns with variable spacing and 130 rows. The block is simulated by a Bingham body with an infinite yield τ_0 and without erosion–diffusion $D = 0$.

The numerical profile of the slide at times $t = 0{\cdot}5$ and 1·0 s (Figure 1) shows that the block conserves its shape except for a slight numerical diffusion of the angle. The vertical displacement of the block calculated by the model can be compared with the experimental vertical displacement (Fig. 2). Few differences can be observed. After an acceleration phase lasting 0·4 s, the block attains an average vertical speed of 0·61 m/s. The end of the fall occurs at a time close to $t = 1{\cdot}0$ s. In the experiment, the block reaches the bottom at $t = 0{\cdot}97$ s. The profile of the free surface obtained numerically is compared with the experimental profile in Figure 3 at times $t = 0{\cdot}5$ s and 1·0 s. At $t = 1{\cdot}0$ s a wave is observed with a peak-to-trough amplitude of approximately 30 cm. The origin of the axes is located at the free surface vertically of the upper right corner of the rigid block. The trough of the wave is due to the fact that the block draws water with it as it falls. The water is then pushed back by the vertical face of the block and fills the trough. The small differences observed near the block ($-0{\cdot}5$ m $< x < 0$ m), immediately above the block, can be explained by the formation of a local vortex at the same place in the experiment.

It is thus possible to model a rigid body in this hydrodynamics program. Furthermore, the tank experiment is correctly modelled: the dynamics of the slide and the amplitude of the wave are reproduced by the numerical model, i.e. by a direct calculation taking into account the interaction of the slide with the ambient environment.

This program is thus able to simulate the submarine slide of a rock mass and evaluate the generated water waves. We can now examine some more complex rheological soils like sand.

5. SMALL-SCALE SANDFLOWS AND WATER WAVES

Channel experiments[12] were conducted in December 1994 with the collaboration of the CEMAGREF (Centre National du Machinisme Agricole du Génie Rural des Eaux et des Forêts, Grenoble, France) in order to test sand submarine landslides.

These experiments consist in generating water waves by allowing a mass of sand to slide freely down a frictionless inclined plane with a slope of 45°. The channel is 4 m long, 0·30 m wide and 2 m high. Two materials are used, a coarse gravel with a grain size between 2 and 7 mm and a fine

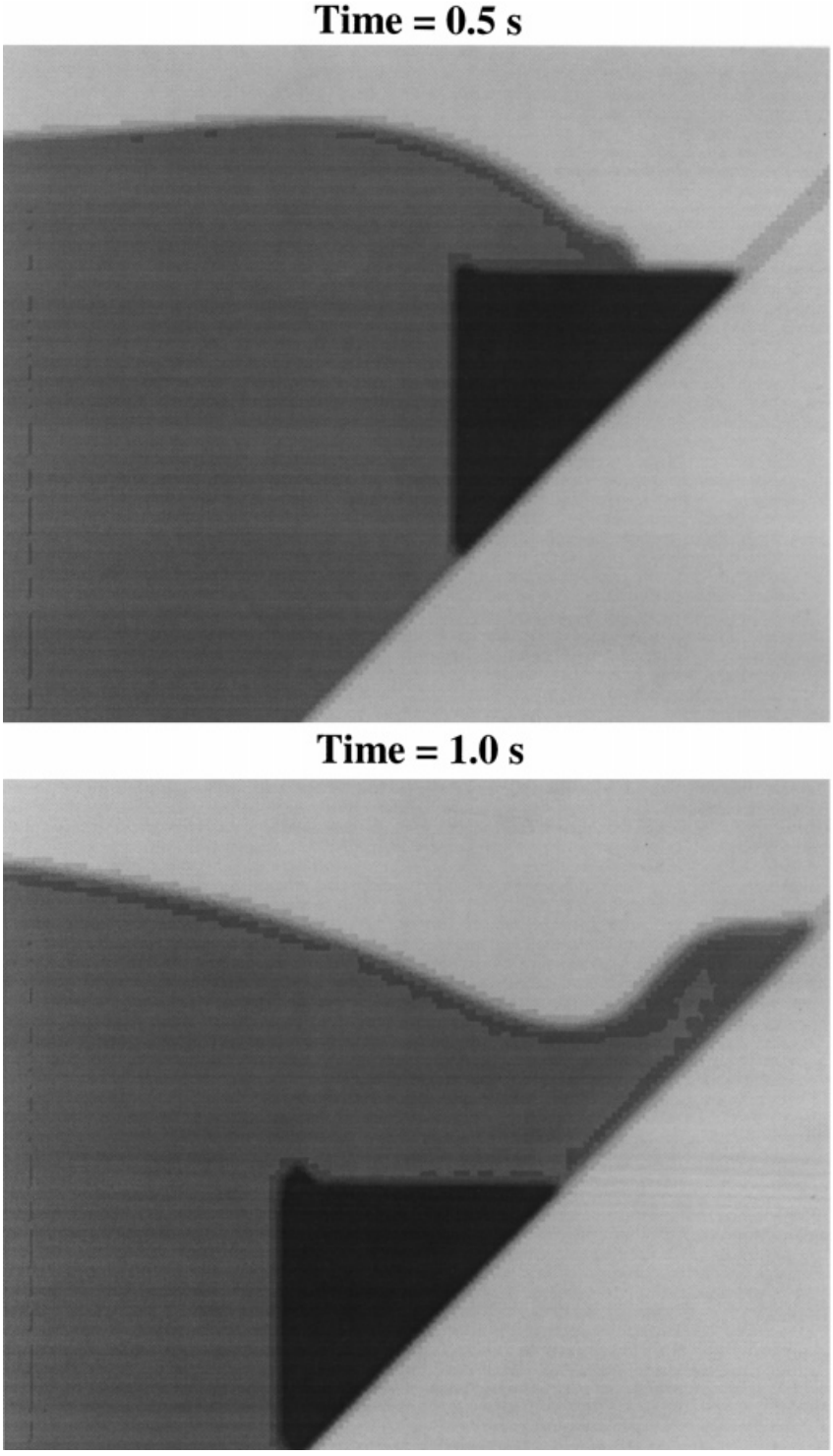

Figure 1. Numerical rock slide test (Size 1·5 m × 1·2 m)

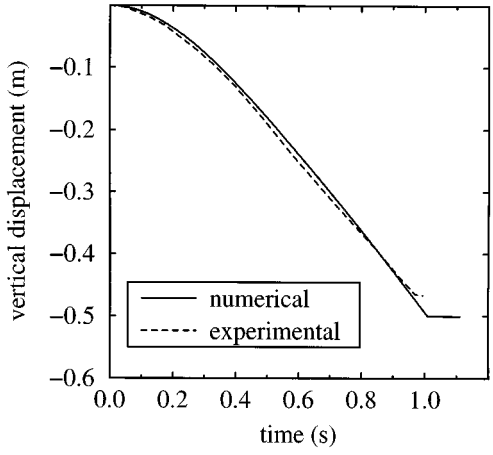

Figure 2. Numerical and experimental vertical displacement of the block

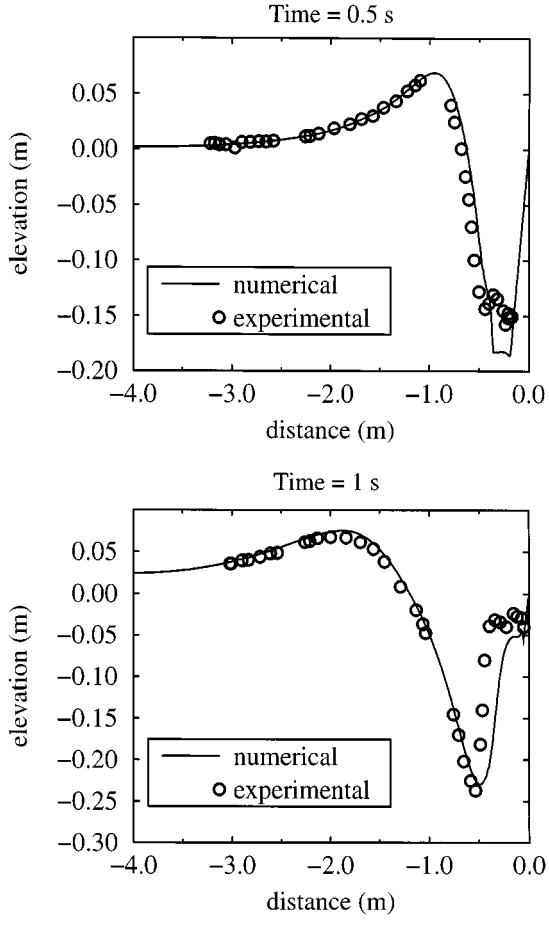

Figure 3. Numerical and experimental free surface for the rock slide test

sand with a grain size between 0·05 and 0·25 mm. The initial vertical profile of the granular mass is triangular. This triangular shape is not realistic in comparison with natural slides but is chosen for simplifying the experiment. The cross-section dimensions of this mass are 0·65 m × 0·65 m. The mass, with a volume of 63 dm^3, is held in its initial position by a vertical water gate. This gate is lifted up quickly at $t = 0{\cdot}0$ s. The mixture density is 1·95, corresponding to a porosity of $n = 42\%$. Thus both materials are loose. The granular materials are put in place progressively to avoid any heterogeneity. The water depth is 1·60 m and the top of the triangular mass is initially 10 cm below the water surface. Figures 4, 5, 10 and 11 show theses experimental slides for the coarse gravel and for the fine sand.

5.1. Consolidation theory and interpretation of the experimental tests

Previously, the soil was assumed to consist of a single phase, and the effect of interstitial water on rheological behaviour was neglected. The water-saturated soil is now considered as two-phase material consisting of an interstitial fluid and a solid skeleton.

According to the principle of Terzaghi,[13] the effective stress tensor alone governs the behaviour of the solid skeleton and is expressed as follows:

$$\begin{aligned} \sigma' &= \sigma - u\mathbf{I} \\ \tau' &= \tau \end{aligned} \tag{15}$$

σ and τ are the total stress tensor and the total stress deviator in the x, y plane, σ' and τ' are the effective stress tensors, u is the pressure of the interstitial fluid and $\mathbf{I}$ the two-dimensional identity tensor.

For a water-saturated soil, the bulk modulus of the solid skeleton being much smaller than that of water, the volume change is related to the interstitial pressure under undrained conditions by the expression[14,15]

$$\Delta V = -\frac{nV}{K}\Delta u \tag{16}$$

where K is the bulk modulus of the water and n the porosity. The volume change therefore results in a pressure change. Consequently, the deformation of the material is coupled to the change in interstitial pressure.

In particular, in a saturated medium, after rapid loading, the interstitial water is loaded. This water moves obeying Darcy's law and gradually the load is transmitted to the solid skeleton. Eventually, the interstitial overpressure vanishes.

The water expulsion phenomenon is described by the consolidation or interstitial pressure diffusion equation[15]

$$\frac{\partial u}{\partial t} - C_{\mathrm{v}}\nabla\cdot(\nabla u - \rho_{\mathrm{w}}\mathbf{g}) = 0 \tag{17}$$

where C_{v} is known as the consolidation coefficient.

The coefficient C_{v} is proportional to the permeability coefficient k, which has the dimension of a velocity and defines the physical filtration property. For sands,[14] this permeability is proportional to the square of the grain diameter d_{10}. Thus, the permeability decreases rapidly with the size of grains.

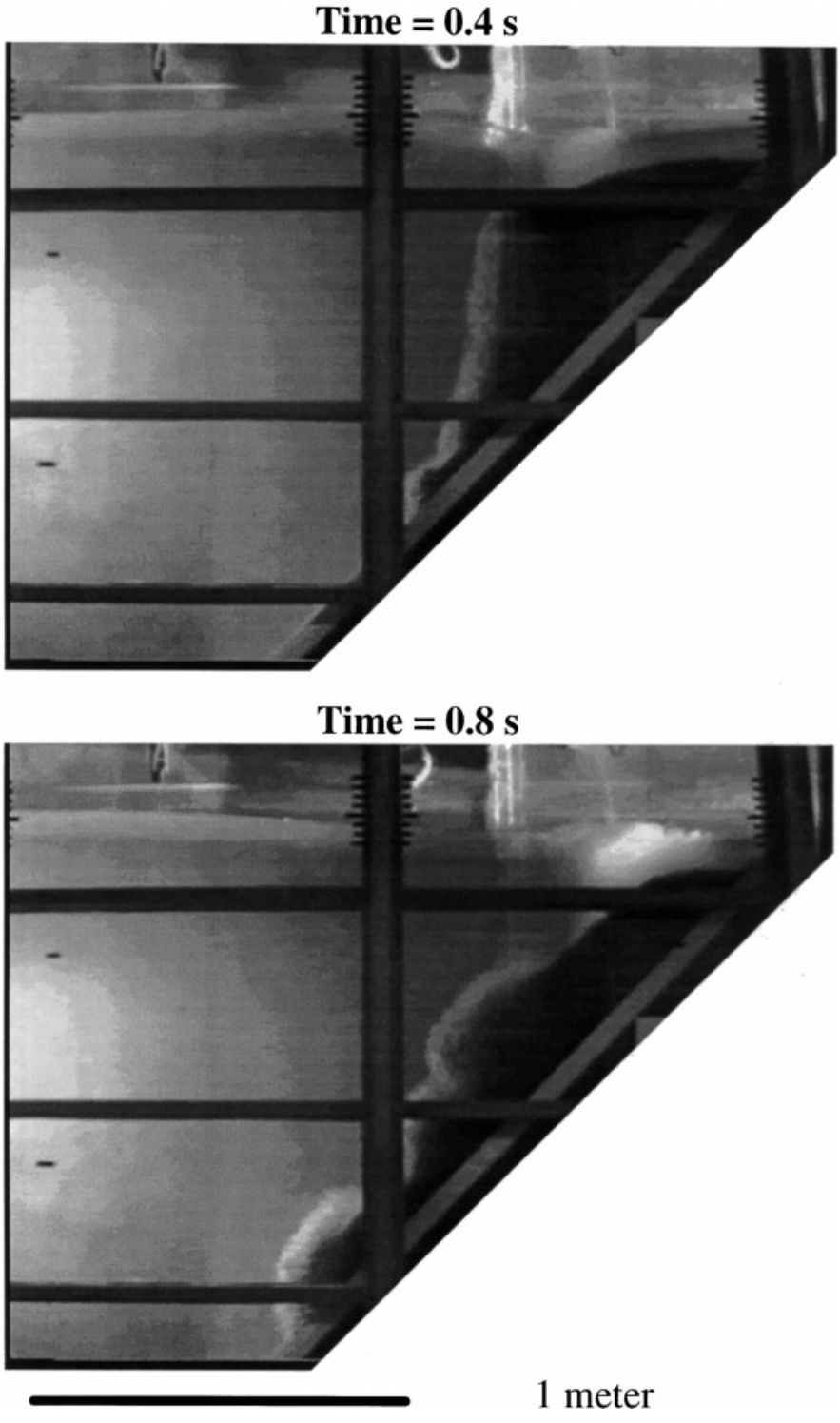

Figure 4. Experiment on coarse gravel, $t = 0{\cdot}4$ and $0{\cdot}8$ s

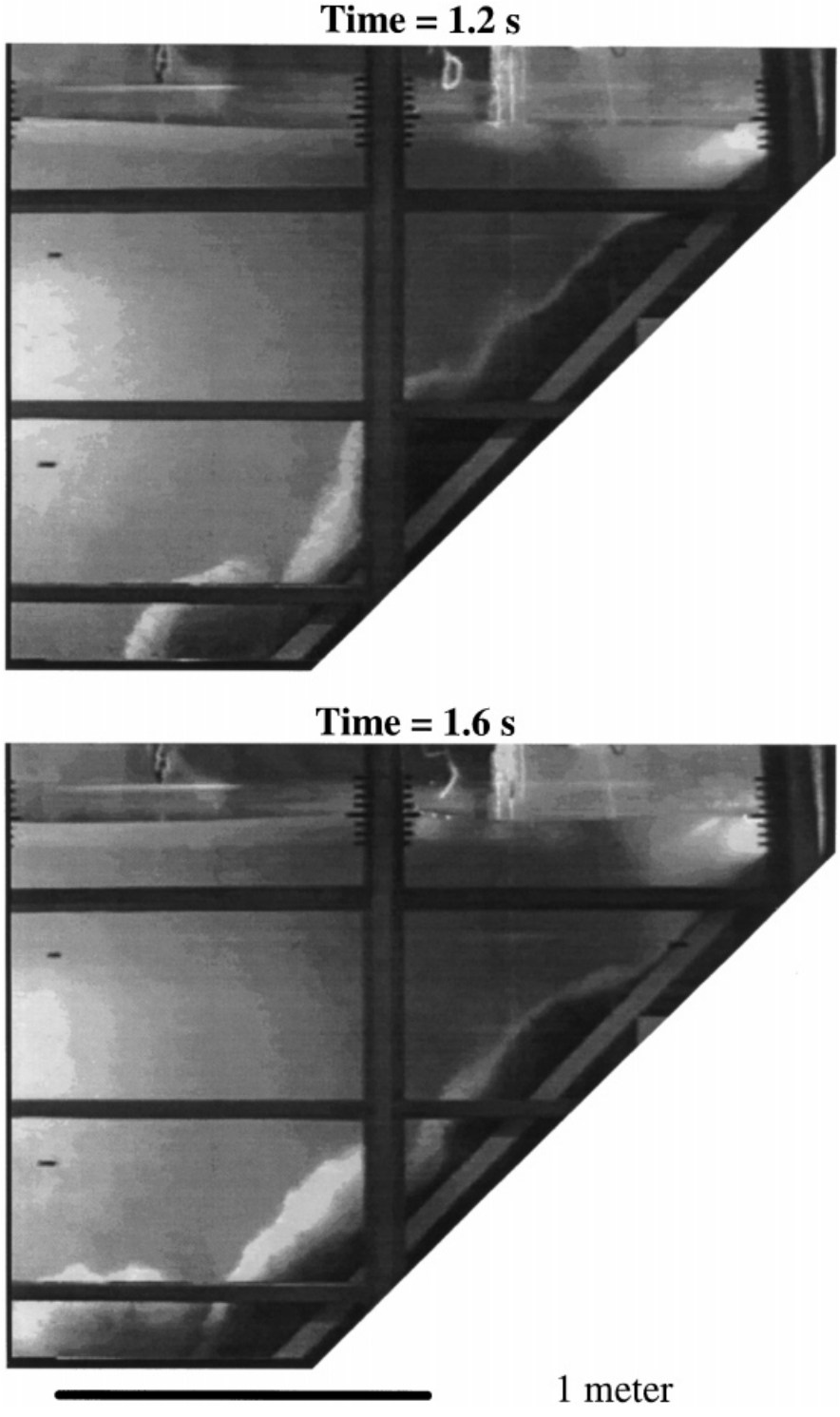

Figure 5. Experiment on coarse gravel, $t = 1{\cdot}2$ and $1{\cdot}6$ s

For a given material, in the one-dimensional elastic theory of consolidation, the time necessary to attain a certain degree of consolidation is proportional to the square of the thickness l of the compressible layer, and depends on the consolidation coefficient (and therefore on the grain size distribution of the material). The characteristic time of the interstitial pressure diffusion phenomenon is given by the following expression:

$$\text{characteristic time} = \frac{l^2}{C_v} \tag{18}$$

This diffusion phenomenon allows us to interpret the tests. Before the gate is lifted, the interstitial fluid is in equilibrium with the ambient medium and the stress tensor may be defined by the following expressions:

$$\sigma_y = (\rho_{sat} - \rho_w)gh + u \tag{19}$$

$$\sigma_x = K_0(\rho_{sat} - \rho_w)gh + u \tag{20}$$

$$u = \rho_w gh \tag{21}$$

$$0 \leqslant h \leqslant 0{\cdot}65 \text{ m} \tag{22}$$

where h is the depth and K_0 is the effective stress ratio.

At the instant the gate is removed, the transient regime is undrained; the sand then has an apparent cohesion C_u. In each layer of sand, there is an instantaneous change of the total horizontal stress $\Delta\sigma_x$ and interstitial pressure Δu without variation of the total vertical stress σ_y. The total horizontal stress is also equal to the water pressure of the tank.

The stress tensor is

$$\sigma_x = \rho_w gh \tag{23}$$

$$\sigma_y = \rho_{sat} gh \tag{24}$$

$$\sigma'_x = -\Delta u \tag{25}$$

$$\sigma'_y = \rho_{sat} gh - \Delta u \tag{26}$$

The variation of the interstitial pressure depends on the variation of stresses and the initial density of the sand. For example, the interstitial pressure will decrease for a dense and dilating sand. Inversely, for a very loose sand the interstitial pressure can increase. Equation (25) shows that the horizontal effective stress is equal to the variation of the interstitial pressure. If there is an increase of the interstitial pressure, there will be a tension in the sand and the failure will be immediate.

Particularly for the small-scale sandflow with the fine sand, the slide takes a long time so there must be an initial decrease of the interstitial pressure. When the gate is lifted up, the interstitial pressure decreases and the diffusion starts. A decompression is then observed: the water from the tank penetrates into the mass. The water uptake can be described by the diffusion equation (17). *A priori*, we can then consider the fracture mechanism as a transient phenomenon linked to the diffusion of the interstitial fluid pressure within the mass, to the grain size of the sand and its initial density. For a given material, the further from the interface between the sand and the ambient medium, the longer the characteristic duration of the phenomenon. This duration increases for smaller grain size. This interpretation can therefore explain the existence of an apparent ocohesion C_u along the inclined plane. As long as the solid skeleton does not undergo

a certain level of drainage, the sand mass cannot start moving (there is no fracture). This approach cannot be used to determine the exact time at which all the sand is moving, because the characteristic length l changes as the slide proceeds, but it does provide an understanding of the time difference between the fracture of the coarse gravel and the fine sand (Table I). The sandflows are in two dimensions and the sand shape is not constant but a characteristic length $l = 32$ cm may be defined by the half-length of the granular mass. The coefficient C_v for the fine sand has been determined experimentally by consolidation tests. But for the coarse gravel, this coefficient is too great to be determined experimentally, it has been evaluated by back-calculation and trial-and-error.

The interstitial pressure diffusion law thus governs the flow characteristics of the sand. A coarser sand (i.e. higher permeability) can flow faster than a fine sand as the interstitial pressure diffusion mechanism operates more rapidly.

5.2. Implementation of interstitial pressure in the Nasa-Vof program

In order to reproduce the tests carried out on a 45° inclined plane with coarse gravel and fine sand, and to verify the soil mechanics approach described above, we have incorporated the notion of interstitial pressure into the Nasa-Vof program.

The Mohr Coulomb fracture criterion is used:

$$\frac{\sigma_1 - \sigma_3}{2} = \left(\frac{\sigma_1 + \sigma_3}{2} - u\right)\sin\varphi \tag{27}$$

The yield stress τ_0 is defined by the undrained cohesion C_u when the sand is plastic

$$\tau_0 = C_u = \frac{\sigma_1 - \sigma_3}{2} = \left(\frac{\sigma_1 + \sigma_3}{2} - u\right)\sin\varphi \tag{28}$$

This yield stress field τ_0 is not necessarily reached by the τ tensor. The total pressure field being determined by the program in each cell of the mesh at a given time, it is possible to find the interstitial pressure field using the previous expression.

Moreover, because of the permeability of the soil, the interstitial pressure obeys the diffusion equation (17).

Therefore, to introduce the interstitial pressure into the model, we first calculate an initial interstitial pressure field at each time step using expression (28) as explained before. Then we use the diffusion equation (17) in order to calculate the changes in interstitial pressure during the time step. Finally, the values of the yield stress field τ_0 are updated using expression (28). This enables the diffusion of the interstitial pressure to be processed via the diffusion of the yield stress τ_0.

Table I. Duration of tests on sand and characteristic consolidation times

Materials $l = 32$ cm	C_v (m^2/s)	l^2/C_v (s)	Time for all the sand to start moving (s)
Fine sand	8×10^{-4}	130	120
Coarse gravel	0·1	1	1·2

5.3. Numerical modelling of the experimental tests—validation

On the basis of the development of the interstitial pressure in the Nasa-Vof program, we can simulate the tests on the sand.

The computational domain is 4 m (-3 m $< x <$ 1 m) by 2 m in the x and y directions. The grid consists of 300 columns with variable spacing and 200 rows. The origin of the axes is located at the free surface vertically of the upper right corner of the granular mass.

The two materials are simulated by a Bingham body with interstitial pressure diffusion. The initial stress state, when the gate is lifted up, is supposed to be slightly under the yield surface, the distance being defined by an arbitrary little constant ($a = 150$ Pa). The initial yield stress field τ_0 is the same for both materials and varies linearly with depth between 150 and 3200 Pa as may be seen from

$$\tau_0 = \frac{\sigma_1 - \sigma_3}{2} + a = \left(\frac{\rho_{\text{sat}} - \rho_{\text{w}}}{2}\right) gh + a \tag{29}$$

The friction angle and the cohesion are determined experimentally $\varphi = 30^\circ$, $C = 0$ and the viscoplasticity $\mu_{\text{b}} = 0$. The consolidation coefficients are different for the two materials, $C_{\text{v}} = 0{\cdot}1\ \text{m}^2/\text{s}$ for the coarse gravel and $C_{\text{v}} = 8 \times 10^{-4}\ \text{m}^2/\text{s}$ for the fine sand.

5.4. Coarse gravel

The numerical profile of the slide is shown using density maps (Figures 6 and 7) at times $t = 0{\cdot}4$, 0·8, 1·2 and 1·6 s.

At time $t = 0{\cdot}8$ s, the yield stress has largely diffused numerically and the soil is considered as a perfect fluid in the model. But, the displacement of the soil near the slope is still small. Figure 8 shows the comparison between the numerical and experimental profiles of the slide. At time $t = 0{\cdot}8$ *s*, the average velocity of the flow (which is approximately that of the front) is 0·8 m/s and the length of the flow is approximately 1·25 m. The fracture mechanism and the flow dynamics are reproduced in a very satisfactory manner at times $t = 0{\cdot}4$ and 0·8 s.

The velocity of the front determined experimentally at the same time is also 0·8 m/s and the length of the flow is 1·35 m/s.

Figure 9 shows the comparison of the numerical and experimental free surfaces at times $t = 0{\cdot}4$ and 0·8 s. At time $t = 0{\cdot}4$ s, a peak amplitude of 1 cm is observed. The maximum amplitude of the trough (at $x = -0{\cdot}44$ m) is 4 cm in the model and 5 cm experimentally. The difference can be explained by the effect of removal of the gate at the start of the slide. In fact, the interstitial pressure diffusion is almost instantaneous. The time required to diffuse over some 10 cms is less than 0·2 s, which is the time required to remove the gate. At time $t = 0{\cdot}8$ s, the wave is relatively well reproduced.

In order to model the formation of the suspension flow characterized by a low density, the next model introduces Fick's law, which enables the concentration to be reduced in a layer close to the interface between the material and the surrounding water. The phenomenon depends on the relative velocity of the two media. As the phenomenon is an interface phenomenon, only the grid cells at the boundary between the sand and the water are concerned. Therefore, beyond a certain threshold velocity $v > v_0$ where $v_0 = 0{\cdot}5$ m/s, the granular material diffuses in the ambient medium $D = 0{\cdot}004$ Pa.s. The threshold value v_0 has been set with respect to time $t = 0{\cdot}4$ s. At this time, the erosion phenomenon is still negligible. The diffusion coefficient D is evaluated by back-calculation and trial and error.

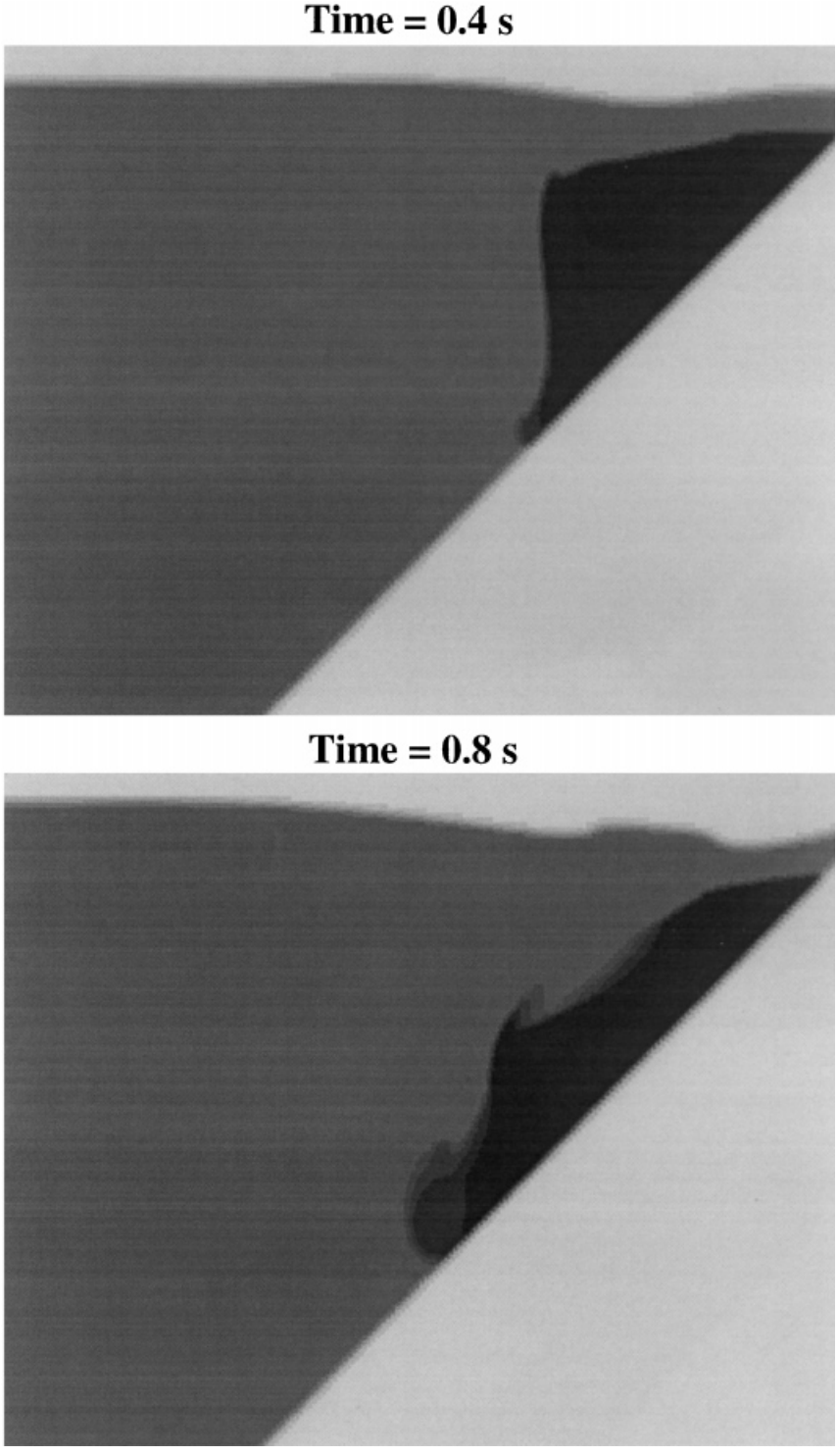

Figure 6. Numerical coarse gravel test (Size 2·0 m × 1·6 m)

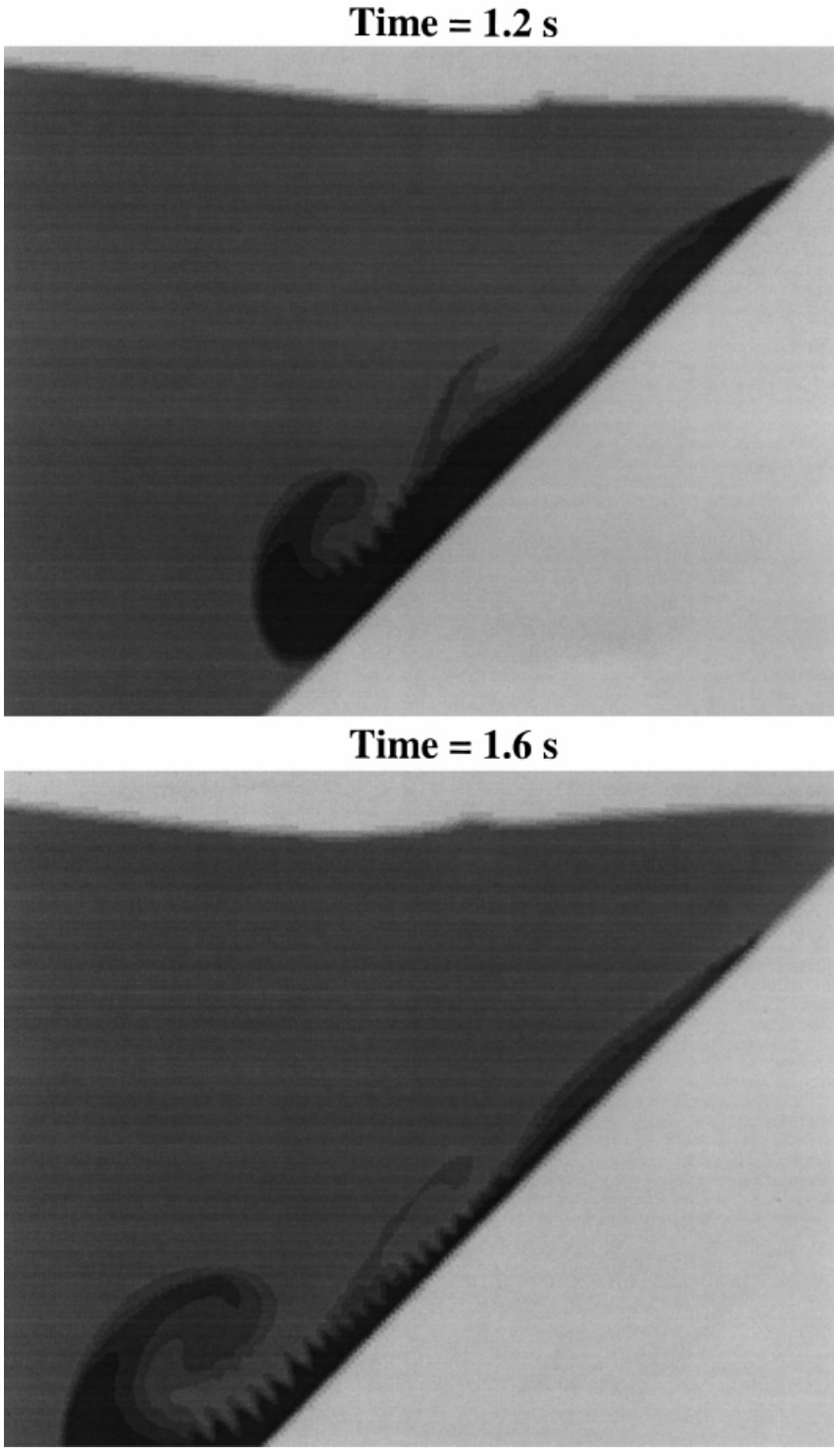

Figure 7. Numerical coarse gravel test (size 2·0 m × 1·6 m)

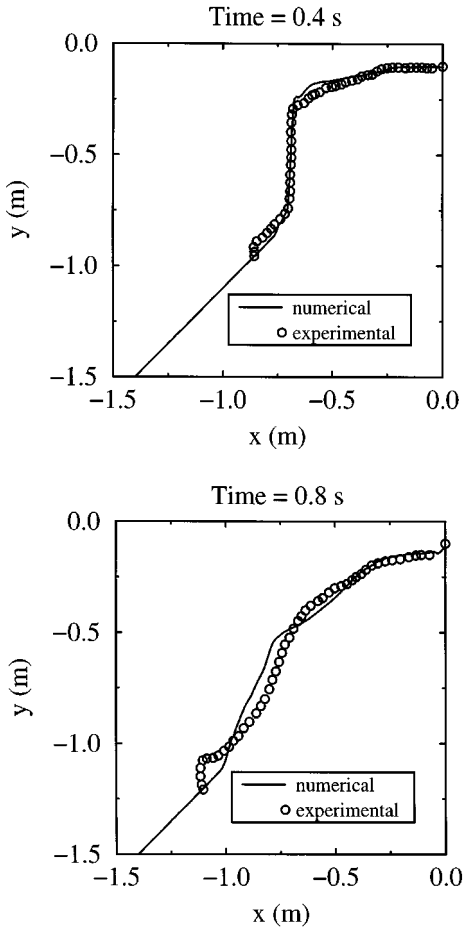

Figure 8. Numerical and experimental profile of the coarse sand

The two vortexes observed in the experimental tests are modelled. At time $t = 1{\cdot}2$ s, a dense part of the flow is observed along the slope and a low-density part at the surface of the slide and at the flow front. At the slope break (at time $t = 1{\cdot}6$ s), the high-density part increases in volume and the hydraulic jump observed in the experiments is reproduced in a satisfactory manner (Figure 7). Despite its simplicity, the diffusion model has been considered in order to verify its capability to simulate the creation of turbidity current.

5.5. *Fine sand*

Fine sand is used. Figures 10 and 11 show the test at time $t = 0{\cdot}0$, 30·0, 50·0 and 105·0 s. After approximately 2 min, a part of the sand mass has not slid. The slide occurs by gradual fractures that develop from the bottom of the pile of sand upwards. For example, at time $t = 50{\cdot}0$ s the appearance of a fracture surface can be observed within the granular mass. At this time

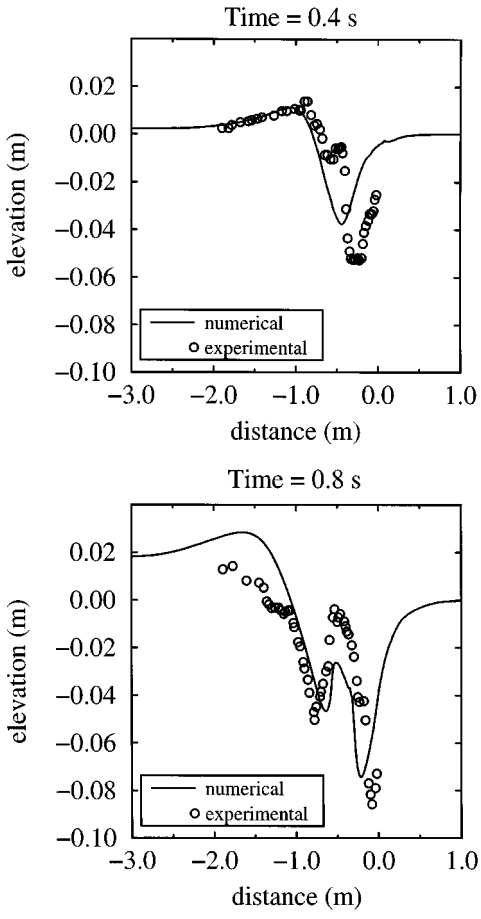

Figure 9. Numerical and experimental free surface for the coarse sand test

the volume of sand that is sliding is small compared with the total volume. The unloading due to the removal of the gate initially affects the interstitial water, and is then gradually transferred to the solid skeleton of the medium. The rapidity of this transfer depends on the permeability of the soil considered. For fine sand this transfer is not instantaneous, which explains the formation of several slide lobes over time.

Figure 12 shows the profile of the slide given by the calculation at times $t = 30{\cdot}0$ and $105{\cdot}0$ s in comparison with the experimental data. The free surface has been very slightly disturbed by the sliding of this type of material. No wave has been generated, as the flow velocities and the volumes involved in the various phases are too low. The numerical model gives approximate estimates of the volume of sand that has not flowed at times $t = 30$ and 105 s and that remains at the top of the inclined plane in its initial position.

The numerical modelling of these two tank tests further validates the model and confirms the hypothesis of the effect of the interstitial pressure on the behaviour of the granular mass.

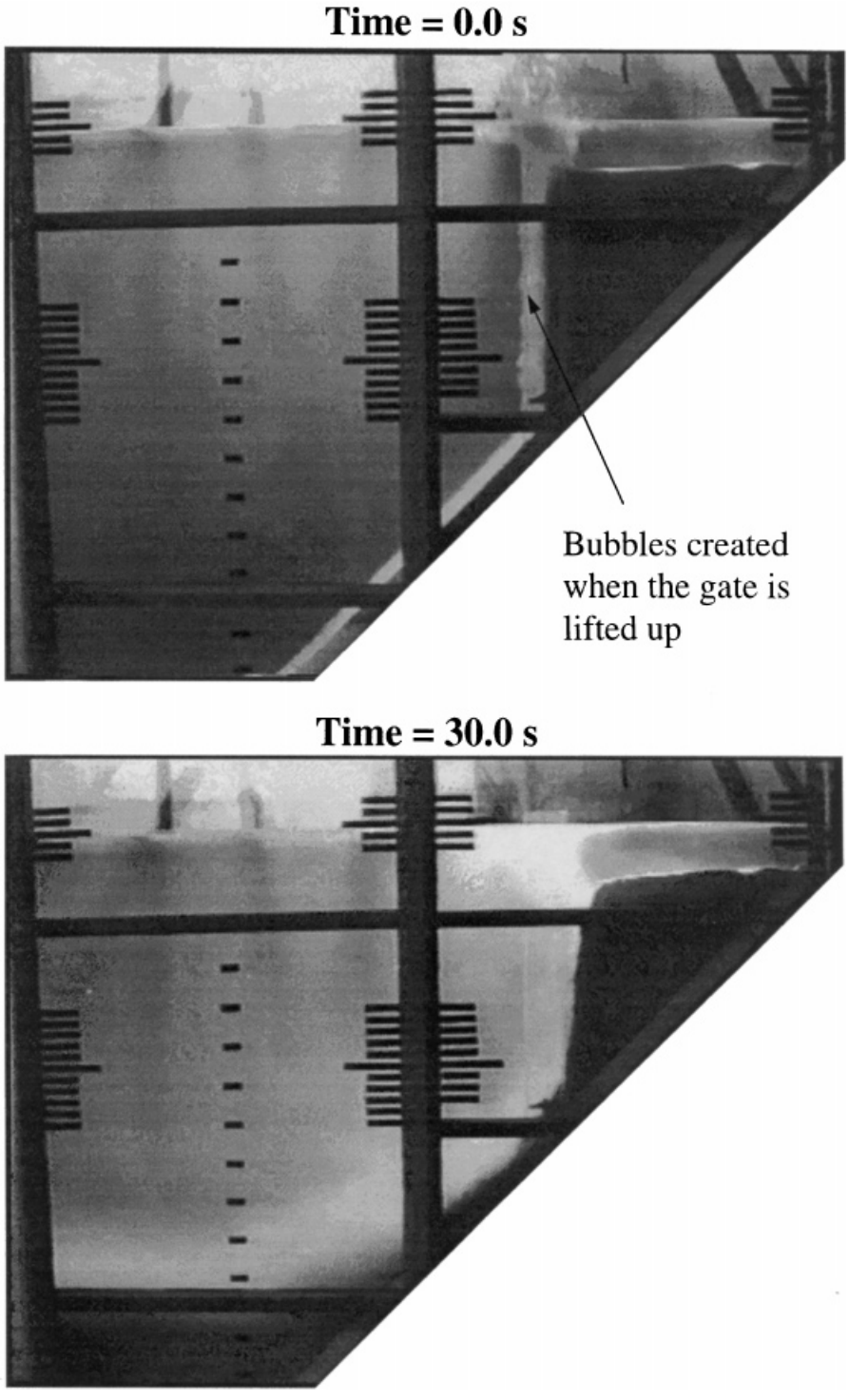

Figure 10. Experiment on fine sand, $t = 0$ and 30 s (size 2 m × 2 m)

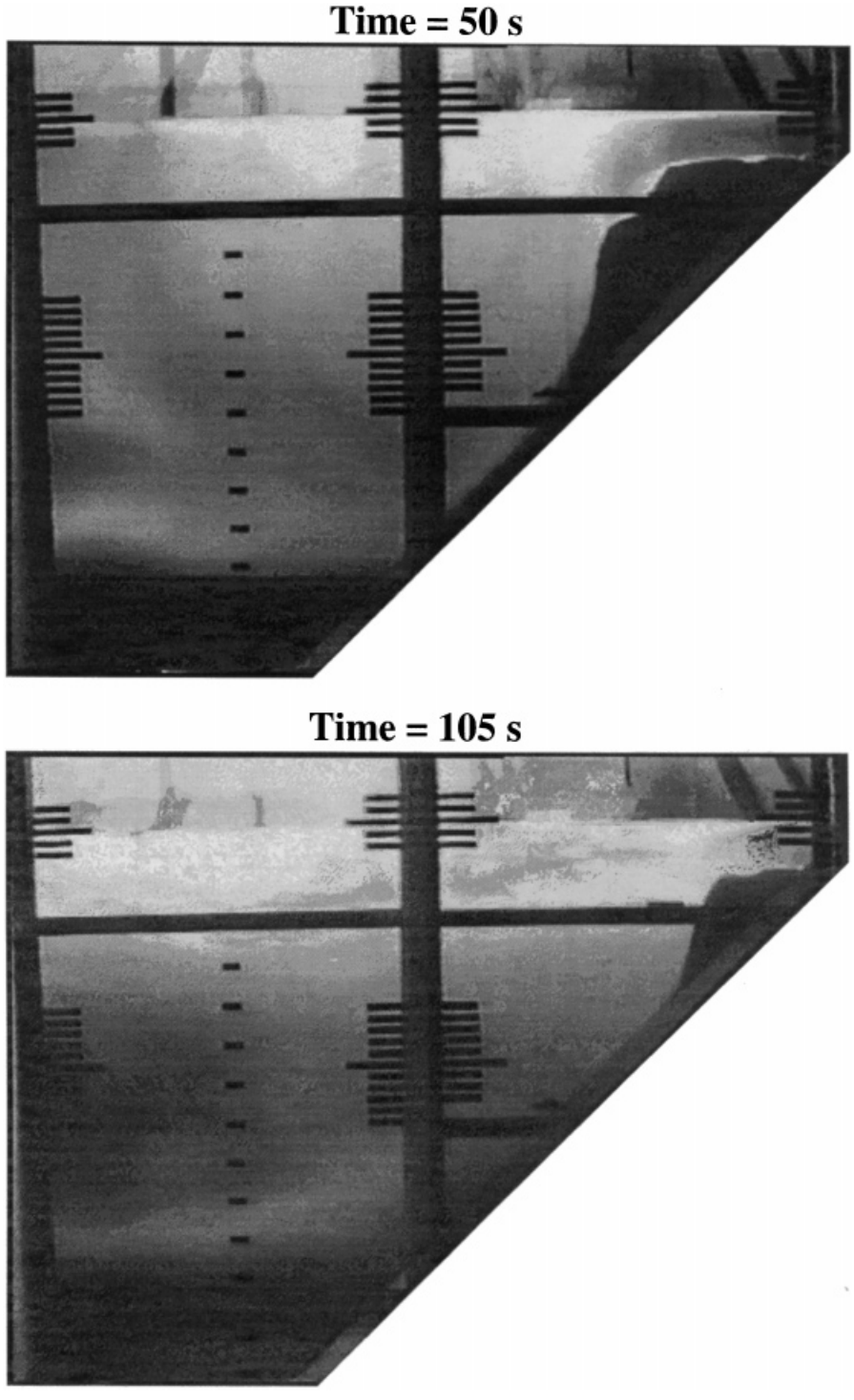

Figure 11. Experiment on fine sand, $t = 50$ and 105 s (size 2 m $\times$ 2 m)

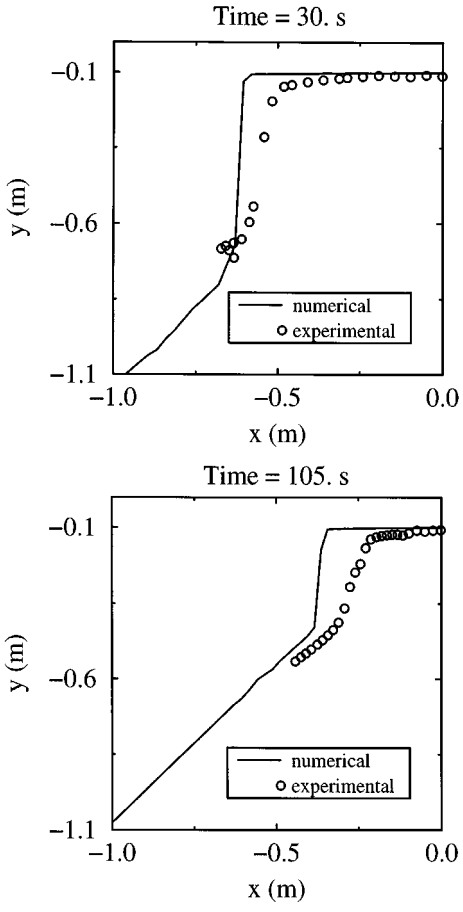

Figure 12. Numerical and experimental profile of the fine sand

6. CONCLUSION

A Navier–Stokes 2D program has been modified to process the mechanical behaviour of sediments by introducing Bingham's law. These initial modifications enabled perfect reproduction of a falling block in water, simply by imposing initial conditions. In order to reproduce submarine slide tests on two granular materials, a second series of modifications was made to the program by introducing interstitial pressure with diffusion in the sedimentary part and an sediment erosion–diffusion law at the water–soil interface. These modifications enabled the reproduction of tests on two granular materials with very different permeabilities. These experiments have revealed the very important role of the interstitial water, which governs the velocity of the slide according to the characteristic consolidation time of the sediments. The erosion–diffusion mechanism provides coarser reproduction of the final phase of the slide, which enters a turbulent and purely hydraulic regime. The importance of the rheology of the sediments and of the interstitial pressure on the slide velocity, and consequently on the height of any waves

that might be generated, can thus be demonstrated. These results suggest further developments and studies, including a full-scale study on an actual slide and a development of the diffusion–erosion law to better model the final phase of the slide.

ACKNOWLEDGEMENTS

This research has been financed by the DG XII of the Commission of the European Communities within the framework of the project GITEC (Genesis and Impact of Tsunamis on European Coasts).

REFERENCES

1. J. G. Moore, 'Giant submarine landslide on the Hawaiian Ridge', *Geological Survey Res.* **501-D,** D95–D98 (1964).
2. H. J. Lee, 'Evidence of rapid gravitational mass movement on the submerged flanks of the Hawaiian Islands', '*Pierre Beghin*' *International Workshop on Rapid Gravitational Movements*, Organized by the CEMAGREF in Grenoble, 1993.
3. E. Jansen, S. Befring and T. Bugge 'Large submarine slides on the Norwegian continental margin: sediments, transport and timing', *Marine Geol.*, **78,** 77–107 (1987).
4. E. A. Kulikov, A. B. Rabinovich, R. E. Thomson and B. D. Bornhold, 'The landslide tsunami of November 3, 1994, Skagway Harbor, Alaska', *JGR Oceans*, **103** (C3)**,** 6609–6615 (1996).
5. L. Jiang and P. H. Leblond, 'The coupling of a submarine slide and the surface waves which it generates', *J. Geophys. Res.* **97** (12)**,** 731–744 (1992).
6. M. D. Torrey, L. D. Cloutman, R. C. Mjolness and C. W. Hirt, NASA-VOF2D: A computer program for incompressible flows with free surfaces, *Report LA-10612-MS*, Los Alamos, NM, 1985.
7. L. Ishii, *Thermo-fluid Dynamic Theory of Two-Phase Flow*, Published by Eyrolles, Paris, 1975.
8. I. R. Ellul, The prediction of dispersed gas–liquid flow in complex pipe geometries, *Doctoral Thesis*, University of London, 1989.
9. P. Nielsen, 'Suspended sediment concentration profiles', *Appl. Mech. Rev.*, **48** (9)**,** 564–569 (1995).
10. A. Huerta and W. K. Liu, 'Viscous flow with large free surface motion', *Comput. Meth. Appl. Mech. Engng*, **69,** 277–284 (1988).
11. P. Heinrich, Etude numérique et expérimentale des vagues générées par des effondrements de terrain, *Thesis*, Ecole centrale de Paris, France, 1992.
12. S. Assier-Rzadkiewicz, Etudes numériques et expérimentales d'un glissement de sédiments le long d'une pente sous-marine et des vagues générées, Thesis, Université de Montpellier II, France (1997).
13. K. Terzaghi, 'The shearing resistance of saturated soils and the angle between the planes of shear', *Proc. 1st Int. Conf. on Soil Mech. and Found. Engr.*, Harvard University, Vol. I, 1936, pp. 54–56.
14. Y. Guéguen and V. Palciauska, *Introduction à la physique des Roches*, Hermann Science and Arts Publishers, 1992.
15. J. Costet and G. Sanglerat, *Cours pratique de mécanique des sols*, Editions Dunod, Paris, 1975.

